Free energy landscapes of electron transfer system in dipolar environment below and above the rotational freezing temperature

Yohichi Suzuki and Yoshitaka Tanimura
Department of Chemistry, Kyoto University, Oiwakecho, Kitashirakawa, Sakyoku, Kyoto 606-8502, Japan

(Received 3 November 2006; accepted 7 December 2006; published online 1 February 2007)

Electron transfer reaction in a polar solvent is modeled by a solute dipole surrounded by dipolar molecules with simple rotational dynamics posted on the three-dimensional distorted lattice sites. The interaction energy between the solute and solvent dipoles as a reaction coordinate is adopted and free energy landscapes are calculated by generating all possible states for a 26 dipolar system and by employing Wang-Landau sampling algorithm for a 92 dipolar system. For temperatures higher than the energy scale of dipole-dipole interactions, the free energy landscapes for the small reaction coordinate region have quadratic shape as predicted by Marcus [Rev. Mod. Phys. **65**, 599 (1993)] whereas for the large reaction coordinate region, the landscapes exhibit a nonquadratic shape. When the temperature drops, small notched structures appear on the free energy profiles because of the frustrated interactions among dipoles. The formation of notched structure is analyzed with statistical approach and it is shown that the amplitude of notched structure depend upon the segment size of the reaction coordinate and is characterized by the interaction energy among the dipoles. Using simulated free energy landscapes, the authors calculate the reaction rates as a function of the energy gap for various temperatures. At high temperature, the reactions rates follow a bell shaped (inverted parabolic) energy gap law in the small energy gap regions, while it becomes steeper than the parabolic shape in a large energy gap regions due to the nonquadratic shape of the free energy landscape. The peak position of parabola also changes as the function of temperature. At low temperature, the profile of the reaction rates is no longer smooth because of the many local minima of the free energy landscape. © *2007 American Institute of Physics*. [DOI: 10.1063/1.2431172]

I. INTRODUCTION

The free energy landscape of electron transfer (ET) system is of fundamental importance to account for ET rates in solvent as recognized by Marcus.[1,2] In this context, the free energy landscapes of the reactant and product are expressed in terms of a reaction coordinate consisting of reactant and product along with their surrounding of solvent. Marcus evaluated the free energy of a given polarization and calculated the ET reaction rates as

$$k \sim \exp\left(-\frac{(\lambda+\Delta G)^2}{4k_B T\lambda}\right), \tag{1.1}$$

where λ and $-\Delta G$ are the reorganization energy and the energy gap, respectively. From the above expression (the energy gap law), Marcus predicted the inverted parabolic (bell shaped) dependence of ET rates as the function of energy gap indicating that the ET rates increase in the small energy gap region (the normal region), whereas they decrease in the large energy gap region (the inverted region). His expression was based on a continuum dielectric model of solvent and thus the molecular aspects of the solvent were missing.

Although Marcus's theory explained the energy gap dependence reasonably well,[3–5] such macroscopic continuum model is not sufficient to describe ET processes especially for dynamics of solvent.[6] The free energy landscapes of the macroscopic dielectric system were given by a functional form of polarization.[2,7] To calculate the free energy landscape using models based on the microscopic molecular details, one has to define relevant reaction coordinate. Taking statistical mechanics approach, Marcus explored ways of abstracting to small dimensional coordinates from the multidimensional phase space using the technique of equivalent equilibrium distribution.[8] His idea was later developed and utilized for the calculation of the ET rate by computer simulations.[9] Calef and Wolynes showed that a reaction coordinate could be adequately defined by the microscopic interaction energy,[10] and several computer simulations were carried out using the reaction coordinate which have energy dimension to confirm the legitimacy of Marcus's theory.[11–14] An expression of the free energy in terms of molecular distribution function including dipole interactions was also given by using a density functional theory.[15,16]

Here, we introduce a function $f(\{R_i\})$ for configuration coordinates of solvent $\{R_i\}$ as

$$f(\{R_i\}) \equiv E^R(\{R_i\}) - E^P(\{R_i\}), \tag{1.2}$$

where $E^i(\{R_i\}) \equiv E^i_{d\text{-}s}(\{R_i\}) + E^i_{s\text{-}s}(\{R_i\})$ is the interaction energy for reactant $(i=R)$ or product $(i=P)$ consisting the solvent-solute interaction energy, $E^i_{d\text{-}s}(\{R_i\})$, and solvent dipole-dipole energy $E^i_{s\text{-}s}(\{R_i\})$.[17,18] If we define the free energy landscapes of reactant and product by

$$G^i(x,T) = -k_B T \ln\left(\int dR_1 \cdots dR_N \delta(x - f(\{R_i\})) \times \exp(-E^i(\{R_i\})/k_B T) \right), \quad (1.3)$$

the free energies of the reactant and product satisfy the relation,

$$G^R(x,T) = x + G^P(x,T). \quad (1.4)$$

Suppose if the free energy landscape is expressed in a quadratic form as

$$G^R(x,T) = ax^2 + bx, \quad (1.5)$$

the ET rates are then evaluated as Eq. (1.1), in which $-\Delta G$ is the energy gap between the two surfaces and $\lambda = 1/4a$.

At the present time, the free energy landscape for ET processes is fairly understood at least at the high-temperature case, where the free energy landscape is well approximated by the parabolic function. At low temperatures, however, it is difficult to calculate the reaction rates, since the solvent molecules have enormous degrees of freedom and there are too many local minima that trap molecular motions to acquire the reliable free energy landscapes. In order to deal with such problem, a simple model is often introduced to reduce the degrees of freedom. For example, if we separate the rotational and translational degrees of freedom of solvent molecules, we can simplify the statistical analysis and facilitate the construction of reliable energy landscapes. Since macroscopic variables such as free energy may not be sensitive to the microscopic details of the interactions, we may still gain valuable information that is necessary to account for a role of solvation. Several studies based on a simple model approach were developed to explore the dynamical aspects of solvation at high temperature. For example, a Brownian dipolar lattice model[19,20] and a self-consistent continuum model[21] were used to investigate dielectric relaxation; the former model consists of point dipoles fixed on a simple cubic lattice and the latter describes the rotational motion of a permanent dipole in a spherical cavity. Ionic solvation was also studied by the Brownian model.[22] Several theories for solvation dynamics were developed[23,24] and are compared with computer simulations.[25–27] These models were sufficiently simple for dynamical simulations, but they still contain too many degrees of freedom to survey the free energy landscapes as a function of macroscopic variables, especially at low temperatures.

In this paper, we take the minimalist model approach proposed by Onuchic and Wolynes[28] to study a possible role of solvent molecules in glassy phase in influencing the electron transfer (ET) or charge transfer (CT) reaction rates. In this approach, the ionic solvation in a polar solvent is modeled by a central charge surrounded by dipolar molecules with rotational dynamics represented by dipoles pointing only the inward and outward directions relative to the ion. The simplicity of this model allows us to thoroughly explore how the energetics of solvation depend on solute charge, solvent dipole, and number of solvent molecules with an aid of random energy model (REM) theory.[29,30] The minimalist model was also applied to investigate the dynamical phase transition in addition to thermodynamic phase transition by utilizing the first passage time idea.[31,32] The extension of the minimalist model to multilayer solvent molecules with all dipole-dipole and charge-dipole interactions were applied to investigate the multiple glassy transitions associated with the freezing of the different solvent layers.[33] Concerning the energy landscapes, Suzuki and Tanimura investigated the free energy landscape of an extended minimalist model consisting of a central charge and surrounding dipoles for the distorted two-dimensional lattice as the function of the polarization.[34] Using the Wang-Landau algorithm they showed that the energy landscape exhibits a symmetric profile described by parabolic and quartic functions of polarization, while it exhibits an asymmetric one due to the contributions of linear and cubic terms that arise from the charge-dipole interactions in the absence and presence of the central charge, respectively. When the temperature dropped, the simulated free energy landscapes were no longer smooth due to the presence of multiple local minima arising from the frustrated interaction among the dipoles.

What follows in this paper is a survey of the free energy landscapes for the minimalist model as the function of x defined by Eqs. (1.2) and (1.3) below and above the freezing temperature. In Sec. II, we explain the model and the reaction coordinate and the Wang-Landau algorithm is outlined to calculate the free energy landscape. In Sec. III, the free energy landscapes for different temperatures are numerically calculated by generating all possible states for a 26 dipolar system and by employing Wang-Landau sampling algorithm for a 92 dipolar system. From the calculated free energy landscapes, the ET reaction rates are also evaluated. The final section is devoted to the conclusion.

II. SIMULATION MODEL AND REACTION COORDINATE

The minimalist model proposed by Onuchic and Wolynes consisted of a charged cavity and a single shell of dipoles that were allowed to point only two directions, toward and opposite to the charged cavity.[28] To adapt this model for ET reaction process, we replace the central charged cavity by a solute dipole moment. Then we configure the solvent dipoles around the solute dipole on the three-dimensional distorted lattice with lattice constant L. Here, we treat all solute-solvent and solvent-solvent interactions explicitly, whereas they were assumed to be random Gaussian interactions in the minimalist model with the REM analysis. The schematic view of our model is depicted in Fig. 1. The solute dipole moment is represented by $\mathbf{z}\mu_d^i$, where $\mathbf{z}$ is the unit vector in the z direction and μ_d^i denotes the magnitude of the solute dipole for the reactant ($i=R$) and the product ($i=P$), respectively. We denote the position of each solvent dipole as $\mathbf{r}_j = \mathbf{a}_j + \delta\mathbf{a}_j$, where $\mathbf{a}_j$ is the jth lattice point vector and $\delta\mathbf{a}_j$ is the random displacement from the lattice point. The magnitude and the direction of the jth solvent dipole are denoted by μ_{solv} and the unit vector $\mathbf{S}_j$, respectively, where $\mathbf{S}_j = \mathbf{r}_j/|\mathbf{r}_j|$. If we introduce the sign operator $\sigma_j = \pm 1$, where the sign depends on whether the dipoles are pointing toward

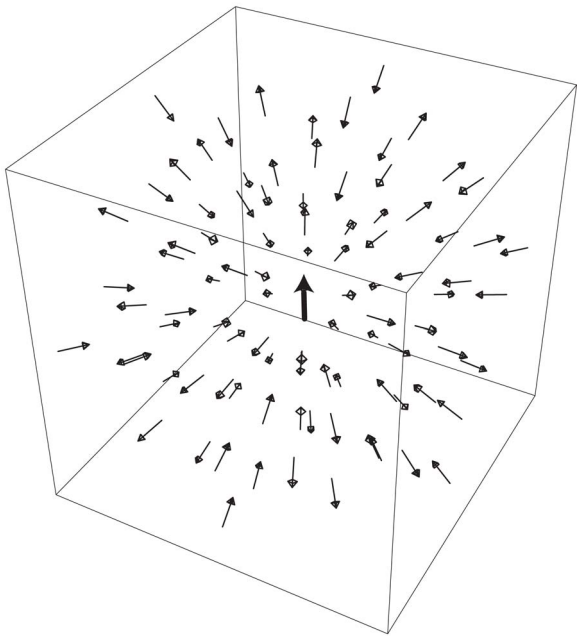

FIG. 1. Schematic view of a solute and solvent model. A solute molecule is represented by a dipole on the center of three-dimensional square lattice. Solvent molecules are expressed by dipoles located on the disordered lattice sites surrounding the central dipoles. Each solvent dipole is allowed to direct only two directions, toward and opposite to the central dipole.

or away from the solute dipole, the dipole moment is expressed as $-\mu_{\mathrm{solv}}\sigma_j\mathbf{S}_j$. Thus all the interactions among solute and solvent dipoles are expressed as

$$E^i(\mu_d^i,\boldsymbol{\sigma}) = E^i_{d\text{-}s}(\mu_d^i,\boldsymbol{\sigma}) + E_{s\text{-}s}(\boldsymbol{\sigma}). \tag{2.1}$$

Here, the energy of the solute-solvent and the solvent-solvent dipoles are defined by

$$E^i_{d\text{-}s}(\mu_d^i,\boldsymbol{\sigma}) = \sum_{j=1}^{N} g_j(\mu_d^i)\sigma_j, \tag{2.2}$$

and

$$E_{s\text{-}s}(\boldsymbol{\sigma}) = \sum_{j=2}^{N}\sum_{k=1}^{j-1} h_{jk}\sigma_j\sigma_k, \tag{2.3}$$

respectively, where

$$g_j(\mu_d^i) = -\mu_{\mathrm{solv}}\mu_d^i \frac{\mathbf{S}_j\cdot\mathbf{z}|\mathbf{r}_j|^2 - 3(\mathbf{S}_j\cdot\mathbf{r}_j)(\mathbf{z}\cdot\mathbf{r}_j)}{|\mathbf{r}_j|^5}, \tag{2.4}$$

and

$$h_{jk} = \mu_{\mathrm{solv}}^2 \frac{\mathbf{S}_j\cdot\mathbf{S}_k|\mathbf{r}_{jk}|^2 - 3(\mathbf{S}_j\cdot\mathbf{r}_{jk})(\mathbf{S}_k\cdot\mathbf{r}_{jk})}{|\mathbf{r}_{jk}|^5}, \tag{2.5}$$

with $\mathbf{r}_{jk}=\mathbf{r}_j-\mathbf{r}_k$ and N is the total number of solvent dipole. This system exhibits a glassy behavior at low temperatures because of the complex interactions among the solvent dipoles with the structural disorder. We chose values typical of ET or CT systems in polar solvents as $\mu_{\mathrm{solv}}=1.85$ and $L=1$ in the unit of Debye and the unit of 2.1 Å, respectively. The characteristic energy is then evaluated as $\Delta U=1.08\times10^{-20}$ J, which is about $2.5(k_BT)$ at room temperature. We employ two types of system: one is $3\times3\times3$ lattice sites and the other is $5\times5\times5$ lattice, but we omit four dipoles on each corner of the lattice for later system due to the limitation of our CPU power. Thus, we used a total of 26 and 92 dipoles for each calculation. We utilize the open boundary condition to avoid undesired effects arise from a treatment of boundary. The displacements from the lattice points obey a Gaussian distribution with average $\langle\delta\mathbf{a}_j\rangle=0$ and standard deviation $\sqrt{\langle\delta\mathbf{a}_j^2\rangle}=0.1$.

For our model we rewrite Eq. (1.2) as

$$f(\boldsymbol{\sigma}) = E^R(\mu_d^R,\boldsymbol{\sigma}) - E^P(\mu_d^P,\boldsymbol{\sigma}). \tag{2.6}$$

The free energy landscapes of the reactant $(i=R)$ and the product $(i=P)$ are calculated from

$$G^i(x,T) = -k_BT\ln\frac{1}{C}\sum_{|f(\boldsymbol{\sigma})-x|<\Delta x}\exp\left(-\frac{E^i(\mu_d^i,\boldsymbol{\sigma})}{k_BT}\right). \tag{2.7}$$

Here, the summation is taken over all configurations for which $f(\boldsymbol{\sigma})$ takes a value between $x-\Delta x/2$ and $x+\Delta x/2$, where Δx is the segment (mesh) size of the reaction coordinate. We introduce the dimensionless constant C to adjust the position of $G^i(x,T)$. When we set C to be proportional to Δx, the position of the energy landscape of different segment size can be fixed if the assigned temperatures are the same. In the following calculations, we set $C=\Delta x/\Delta U$, where $\Delta U=1.08\times10^{-20}$ J is the characteristic energy of the system. In Eq. (2.7), we adopt $\mu_d^R=0$ and $\mu_d^P=2$ for a situation: a neutral solute is surrounded by the solvent in the reactant state and the ET reaction occurs then polarized.

For the 26 dipolar case, we evaluate Eq. (2.7) by generating all configurations of $\boldsymbol{\sigma}$ and classifying $f(\boldsymbol{\sigma})$ in the range $x_i-\Delta x/2\leqslant f(\boldsymbol{\sigma})<x_i+\Delta x/2$ for ith segment x_i, which satisfies $\Delta x=x_{i+1}-x_i$. Although we can obtain the exact free energy landscape for any Δx in such small system, we cannot generate all configurations by any means for a large system. For example, a system with 92 dipoles involves enormous degrees of freedom even with directional restrictions of the dipoles $(\sim2^{92})$. Thus, it is essential to sample relevant states for constructing the free energy landscape. If we can extract a representative subset for states described by energy E and a reaction coordinate x from the all configurations, the free energy landscape can be obtained from the ensemble of the subset. The Monte Carlo method with Metropolis algorithm has been used to generate such representative subsets. However, this algorithm is time consuming for a glassy system at low temperature because the trajectories of the sampled states generated by the algorithm are easily trapped in the local energy minima. To overcome this difficulty, Berg and Neuhaus proposed the multicanonical algorithm,[35,36] which has been applied to many problems such as spin glasses, proteins, and polymers.[37–40] Okumura and Okamoto suggested the multidimensional extensions of the multicanonical algorithm.[41,42] In our previous paper,[34] we demonstrated that the two-dimensional Wang-Landau algorithm[43,44] for energy and polarization states was a reliable and efficient method to have a density of states. Here, we employ the reaction coordinate x defined in Eqs. (2.6) and (2.7) instead of the polarization and adopt the two-dimensional Wang-Landau algorithm to calculate the free energy landscape. The essence of

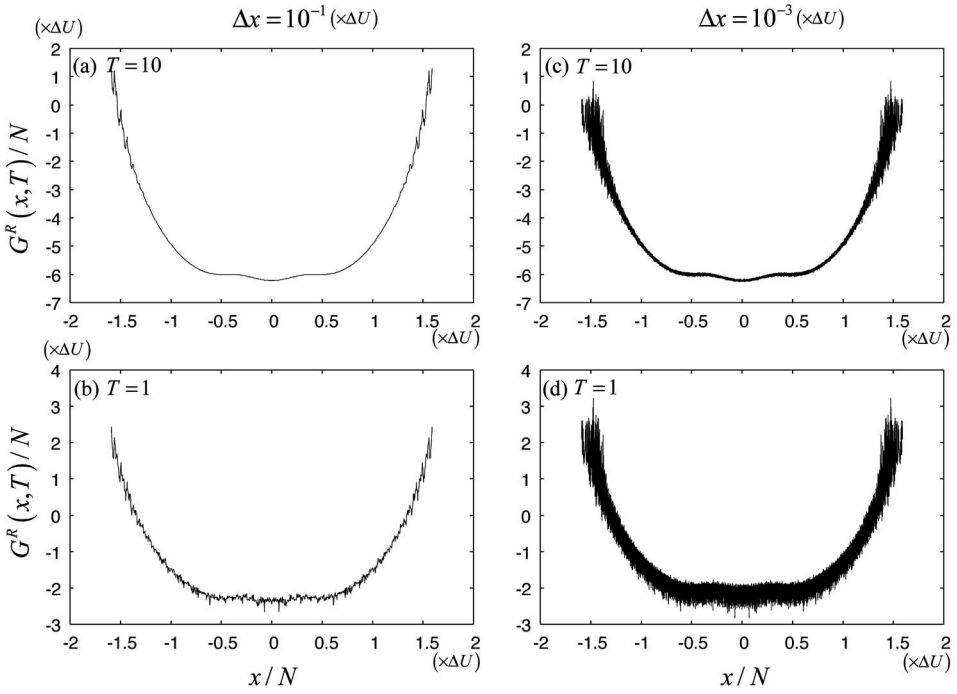

FIG. 2. ; The free energy landscapes of a distorted $3\times3\times3$ square lattice system with 26 dipoles for different temperatures and segment sizes: (a) $T=10$, $\Delta x=10^{-1}$; (b) $T=1$, $\Delta x=10^{-1}$; (c) $T=10$, $\Delta x=10^{-3}$; and (d) $T=1$, $\Delta x=10^{-3}$, respectively. Here, T and Δx are measured in the unit of $\Delta U=1.08\times10^{-20}$ J and we set $k_B=1$.

the algorithm is the uniform sampling in the energy and reaction coordinate spaces by using an artificial sampling weight $g(E,x)$ instead of Boltzmann weight. When the histogram $H(E,x)$ defined by the number of sampled states (E,x) attains larger than 70% of the average value, $\langle H(E,x)\rangle$ for all possible ranges, we regard the sampling as having been done uniformly in the energy and reaction coordinate space. In order to generate the sampling weight, we divide the regions of energy $-2000<E/\Delta U<2000$ and reaction coordinate $-100<x/\Delta U<100$ into 4001 and $(200\Delta U/\Delta x)+1$ segments, respectively. We generate the density of states after obtaining the artificial weight factors by recursive updates which enables us to get a flat histogram of a uniform sampling data in the energy and reaction coordinate spaces. We then calculate the free energy landscape as the function of x by reweighting probabilities to conform to the Gibbs ensemble.

III. RESULTS AND DISCUSSION

A. Free energy landscapes of a 26 dipolar system

Figure 2 illustrates the free energy landscapes of a distorted $3\times3\times3$ square lattice system with 26 dipoles for different temperatures and segment sizes: (a) $T=10$, $\Delta x=10^{-1}$; (b) $T=1$, $\Delta x=10^{-1}$; (c) $T=10$, $\Delta x=10^{-3}$; and (d) $T=1$, $\Delta x=10^{-3}$ in the unit of $\Delta U=1.08\times10^{-20}$ J. Here and hereafter we set $k_B=1$. We analyzed the temperature dependence of the heat capacity and found a sharp peak at $T_c\approx2$ that corresponded to the freezing temperature of dipolar rotational motions. Thus the cases for (b) and (d) are in a glassy state. These landscapes are directly calculated from Eq. (2.7) by generating all possible dipolar states numerically and are not obtained from the Wang-Landau approach. Such exact calculations can be carried out only for a small system with 2^{26} dipolar configurations. We should notice that this system is too small to extract reasonable free energy profiles and we have observed a change of curvature around $|x/N|=0.2$ as an artifact of the small system. Here, we use these results to analyze a role of the segment size of the reaction coordinate, which has to be introduced to calculate the free energy of larger system.

While the free energy landscape becomes smooth at high temperature illustrated in Fig. 2(a), it exhibits small notched structure (roughness) on the profile at low temperature as in Fig. 2(b). This feature can be explained from the distribution of states as a function of reaction coordinate x and energy E as schematically depicted by dots in Fig. 3. At high temperature, all states in the segment between $x_i-\Delta x/2$ and $x_i+\Delta x/2$ contributes to $G^R(x_i,T)$, while only the lower energy part of states in the segment indicated with solid line in Fig. 3 contribute to $G^R(x_i,T)$ at low temperature due to the Boltzmann factor in Eq. (2.7). Since the number of states is

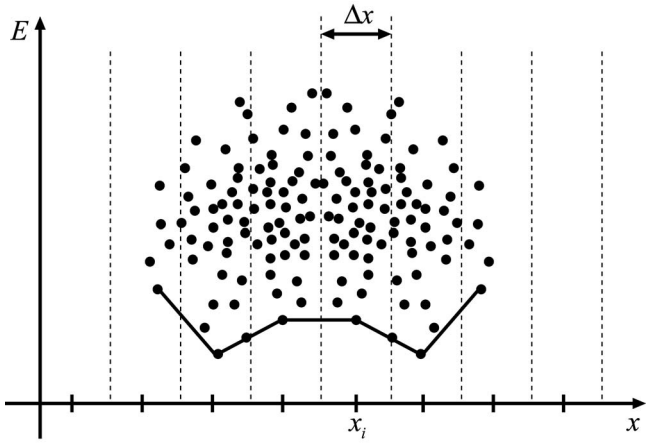

FIG. 3. The dots illustrate the schematic view of the distribution of states as a function of reaction coordinate x and energy E. Solid line represents the lower energy part of states in a segment. The profile of the lower energy part is essential to determine the free energy landscape especially at low temperature.

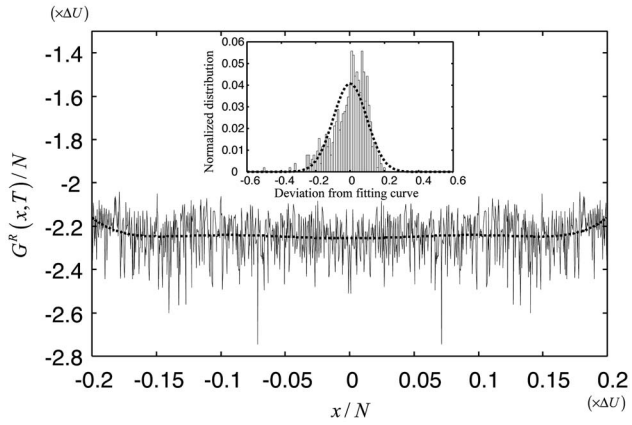

FIG. 4. The free energy landscape (solid line) and fitted curve (dashed line) of a distorted $3\times3\times3$ lattice model for $T=1$, $\Delta x=10^{-2}$. The fitting function is $G^R_{\rm fit}(x)=\Sigma^3_{k=0}a_i(x/N)^{2k}$ with parameters $a_6=6731.75$, $a_4=-307$, $a_2=3.9$, and $a_0=-2.26$. The inset of the figure shows the histogram of $\delta G(x_i)$, which is fitted by the normal distribution (dashed line) with the average $\overline{\delta G}=0.0$ and the standard deviation $\sqrt{\overline{\delta G^2}}=0.098$.

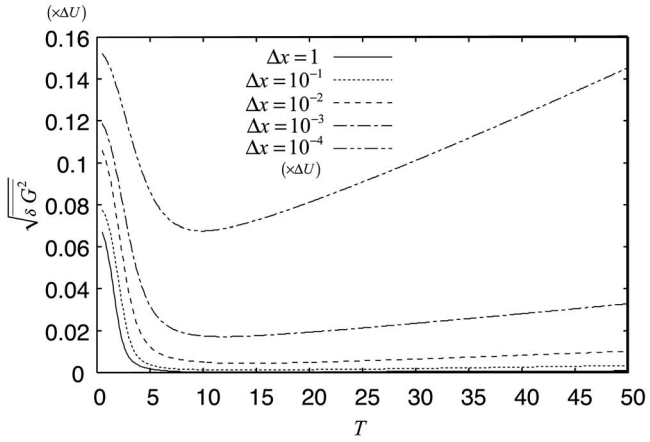

FIG. 5. The standard deviation $\sqrt{\overline{\delta G^2}}$ for the 26 dipolar system as the function of the temperature for various segment sizes.

sparse in the lower energy region, $G^R(x,T)$ changes rapidly as the function of x depending on the position of the low energy states. This feature becomes prominent especially for small Δx, where only a few states can take part for calculations of $G^R(x_i,T)$. In this case, as shown in Fig. 2(c), we also observed the notched profiles of the landscape even at high temperature.

Using the exact distribution of states, we analyzed the statistics of notched structure. First, we extrapolate the profiles of the free energy landscape up to sixth order using the fitting function $G^R_{\rm fit}(x)=\Sigma^3_{k=0}a_{2k}(x/N)^{2k}$ for the range $|x/N|\leqslant 0.2$. Due to the conditions $f(\boldsymbol{\sigma})=-f(-\boldsymbol{\sigma})$ and $E^R(\mu^R_d,\boldsymbol{\sigma})=E^R(\mu^R_d,-\boldsymbol{\sigma})$, $G^R(x,T)$ is symmetric with respect to $x=0$ and the polynomial function does not contain the odd-order terms. Then we subtract $G^R_{\rm fit}(x)$ from $G^R(x,T)/N$ and obtain the notched part of free energy as $\delta G(x_i)=G^R(x_i,T)/N-G^R_{\rm fit}(x_i)$, where x_i is the value of reaction coordinate at ith segment which satisfies $\Delta x=x_{i+1}-x_i$.

Figure 4 illustrates $G^R(x,T)/N$ (solid line) for $T=1$, $\Delta x=10^{-2}$ and the fitted line (dashed line) with the fitting parameters $a_6=6731.75$, $a_4=-307$, $a_2=3.9$, and $a_0=-2.26$. The histogram of $\delta G(x_i)$, which is also fitted by the normal distribution (dashed line) with the average $\overline{\delta G}=0.0$ and the standard deviation $\sqrt{\overline{\delta G^2}}=0.098$, is presented in the inset of Fig. 4. In the small region of x, where the Gaussian fitting works well, we also found that the sequence of $\delta G(x_i)$ is uncorrelated at the different $x_{i'}$ and thus $\delta G(x_i)$ can be regarded as the white noise with respect to x_i.

Calculated $\sqrt{\overline{\delta G^2}}$ as the function of temperature for different Δx is plotted in Fig. 5. The amplitude $\sqrt{\overline{\delta G^2}}$ tends to be large for small Δx, since the number of the states involved in the free energy calculations becomes small and the statistical deviation becomes large. For $T<10$, the amplitude becomes large for small T, since only lower energy states in the segment can contribute to the free energy calculations due to the Boltzmann factor in Eq. (2.7). At very low T, the lowest energy state in the segment dominate the free energy and thus we have $G^R(x_i,T)\approx E_i^{\rm min}$, where $E_i^{\rm min}$ is the lowest energy in the ith segment and therefore the free energy landscapes become temperature independent. For $T>10$, $\sqrt{\overline{\delta G^2}}$ increases as the temperature increases. At such high temperature, the Boltzmann factors play a less role and thus the total number of states in the segment [we denote $n(x_i)$ for the ith segment] determines the value of the free energy as $-k_BT\ln n(x_i)$. Since $n(x_i)$ may change rapidly for small Δx, the amplitude will also change.

In Fig. 6, we plot $\sqrt{\overline{\delta G^2}}/\Delta U$ as the function of $\Delta x/\Delta U$ for different temperatures, where ΔU is the characteristic energy scale of the system. The calculated results can be well fitted by the linear functions in the logarithmic scales. This indicates that we can always extrapolate their amplitudes $\sqrt{\overline{\delta G^2}}$ from the values in large Δx.

Since the lowest energy $E_i^{\rm min}$ determines the free energy in the segment especially in the low temperature case, the differences of the lowest energy among the different segments give rise to the notched structure. To see this point more clearly, we consider the change of total energy and the reaction coordinate for flipping one dipole with others being fixed. The change of the total energy for flipping kth dipole is evaluated as

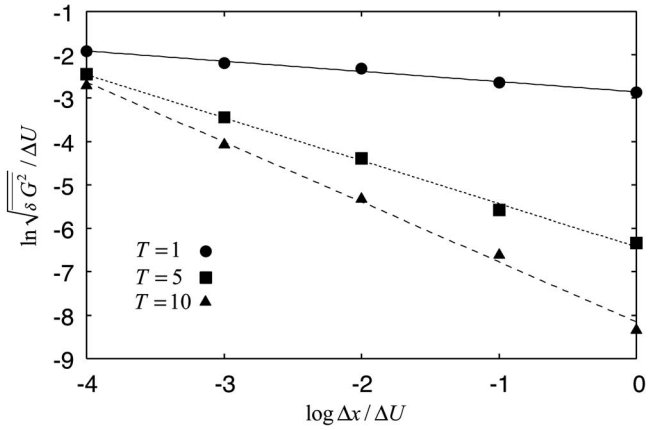

FIG. 6. The standard deviation $\sqrt{\overline{\delta G^2}}/\Delta U$ for the 26 dipolar system as the function of the segment size $\Delta x/\Delta U$, where ΔU is the characteristic energy scale of the system. The calculated results can be well fitted by the linear functions in the logarithmic scales.

$$\Delta E(\sigma_k \to -\sigma_k) = -2\sum_{j\neq k} h_{kj}\sigma_k\sigma_j \approx -2\bar{h}\sigma_k\sum_{j\neq k}\sigma_j, \quad (3.1)$$

where the interaction parameter h_{kj} is approximated by their mean value $\bar{h}$ defined by

$$\bar{h} \equiv \frac{1}{N}\sum_{k=1}^{N}\left(\frac{1}{N-1}\sum_{j\neq k} h_{kj}\right). \quad (3.2)$$

Similarly, the change of reaction coordinate for flipping one dipole is given by

$$\Delta x(\sigma_k \to -\sigma_k) = 2g_k(\mu_d^P)\sigma_k \approx 2\bar{g}\sigma_k, \quad (3.3)$$

where the solute-solvent interaction parameter $g_k(\mu_d^P)$ is approximated by their mean value

$$\bar{g} = \frac{1}{N}\sum_{k=1}^{N} g_k(\mu_d^P). \quad (3.4)$$

If all configurations of $\{\sigma_1,\ldots,\sigma_{k-1},\sigma_{k+1},\ldots,\sigma_N\}$ occur with the same probability, $1/2^{N-1}$, the fluctuation (standard deviation) of total energy and reaction coordinate for flipping one dipole are given by

$$\Delta E_{\text{flip}} = 2|\bar{h}|\sqrt{(N-1)}, \quad (3.5)$$

and

$$\Delta x_{\text{flip}} = 2|\bar{g}|. \quad (3.6)$$

For 26 dipolar system, they are evaluated as $\bar{h}=0.9$ and $\bar{g}=0.05$, respectively, and we have $\Delta x_{\text{flip}}=0.1$ and $\Delta E_{\text{flip}}/N=0.3$. These values are roughly in accordance with the relation in Fig. 6 indicating that the amplitude of the notched structure relates to the flipping energy and the corresponding change of reaction coordinate. We should also notice that although the true free energy landscapes have the notched structures whose scale is much smaller than Δx_{flip}, a real transition may occur only through the flipping of dipoles. Therefore the structure smaller than Δx_{flip} on the free energy landscapes may not affect on reaction processes.

B. Free energy landscapes of 92 dipolar system

Since the number of states is too large to generate for the 92 dipolar system, we sample the states using the Wang-Landau algorithm. We calculate a density of states for the finite segment size Δx and ΔE. In Fig. 7, we present the contour plot of the logarithms of density of state $\ln D(x,E)\Delta x\Delta E$ for $\Delta x=10^{-1}$ and $\Delta E=1$ obtained by the Wang-Landau approach. From the density of states, the free energy landscapes are calculated as

$$G^R(x,T) = -k_BT\ln\frac{1}{C}\int_{-\infty}^{\infty}dE\int_{x-\Delta x/2}^{x+\Delta x/2}dxD(x,E) \times\exp\left(-\frac{E}{k_BT}\right). \quad (3.7)$$

Figure 8 depicts the calculated free energy landscapes of the reactant state $G^R(x,T)/N$ with $\Delta x=10^{-1}$ for different temperatures (a) $T=10$ and (b) $T=1$, respectively. In the same manner as the 26 dipolar system, we estimated the freezing

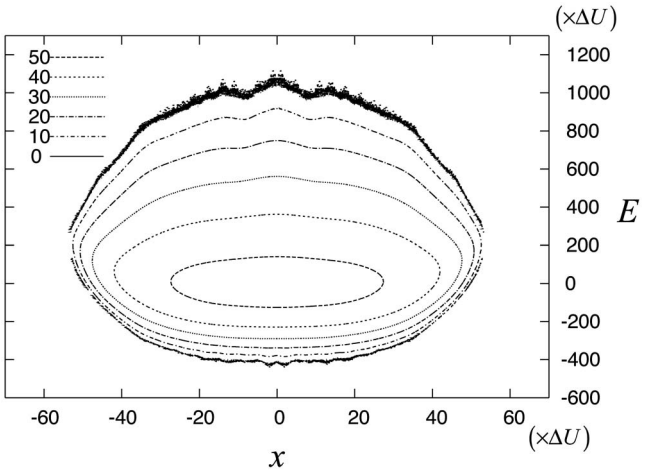

FIG. 7. The contour plot of the logarithms of the density of state $\ln D(x,E)\Delta x\Delta E$ for the 92 dipolar system. The segment sizes of the reaction coordinate and energy are chosen to be $\Delta x=10^{-1}$ and $\Delta E=1$, respectively. The density of states is obtained by the Wang-Landau approach.

temperature at $T_c\approx 4$. The solid lines in Figs. 8(a) and 8(b) are the calculated results, while the dotted lines represent fitting curves with the parabolic function $G(x)=\alpha+\beta(x/N)^2$ for the range $|x/N|\leqslant 0.2$; the parameters are chosen to be (a) $\alpha=-7.7$ and $\beta=5.2$, and (b) $\alpha=-4.6$ and $\beta=5.1$. Note that the presented results are for the specific set of the position

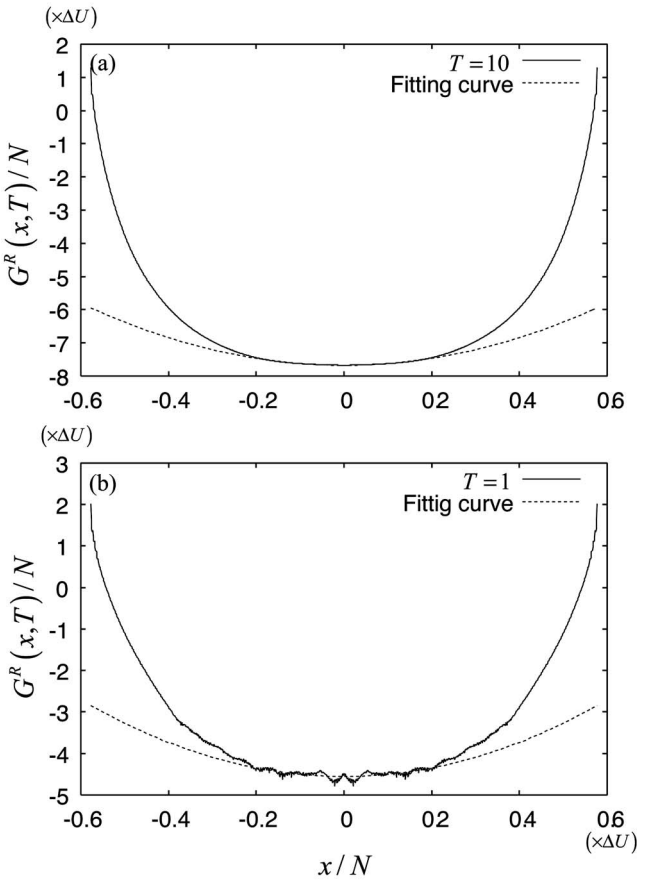

FIG. 8. The calculated free energy landscapes for the 92 dipolar system $G^R(x,T)/N$ with $\Delta x=10^{-1}$ for different temperatures (a) $T=10$ and (b) $T=1$, respectively.

for dipoles and we found that the quadratic region of the free energy landscape may change slightly depending on the distribution of dipoles.

The calculated free energy landscape for the 92 dipolar system at high temperature is depicted in Fig. 8(a). As discussed in the 26 dipole case, the profile of the free energy landscape is governed by the number of states $n(x_i)$ at high temperature. If we assume the energy distribution of states in Gaussian form with the central energy $\bar{E}_i$ and the standard deviation ΔE_i, the free energy is evaluated as

$$G^R(x_i,T) \approx -k_BT \ln \frac{1}{\sqrt{2\pi}\Delta E_i} \int n(x_i) \times \exp\left(-\frac{(E-\bar{E}_i)^2}{2\Delta E_i^2}\right)\exp\left(-\frac{E}{k_BT}\right)dE = -k_BT \ln n(x_i) + \bar{E}_i - \frac{\Delta E_i^2}{2k_BT}, \quad (3.8)$$

where x_i is the ith segment with the region $x_i-\Delta x/2$ and $x_i+\Delta x/2$. Near the minimum of free energy surfaces $|x/N| \leqslant 0.2$, a number of states are involved in $n(x)$ and, based on the central limiting theorem, we can assume Gaussian form for $n(x)$. For high temperature case, the contribution from $-k_BT \ln n(x_i)$ is large and therefore we have the parabolic energy landscapes for $|x/N| \leqslant 0.2$. For large $|x/N|$, however, $n(x)$ contains only a small number of states and $n(x)$ deviates from Gaussian due to the failure of the central limiting theorem. (See also Fig. 7). Consequently, $G^R(x,E)$ shows parabolic and nonparabolic profiles for small and large $|x/N|$, respectively. We should notice that although such feature exists for any system, the deviation from the parabola may be too small to observe in a real system, since it contains tremendous degrees of freedom that make the deviation very small.

Figure 8(b) shows the free energy landscape for $T=1$. In the low temperature case, the free energy landscapes are determined by the lower energy part of distribution $D(x,E)$, because the Boltzmann weight in Eq. (3.7) suppresses the higher energy contributions. Since the lower energy part of $D(x,E)$ is not a smooth function of x as illustrated in Fig. 7, the calculated free energy landscapes at low temperature exhibit notched structure as presented in Fig. 8(b). Following the same procedure as the 26 dipole case, we have extracted the notched part $\delta G(x)$ for all range of x and analyzed their statistics. The amplitude of the notched part of profiles $\sqrt{\overline{\delta G^2}}$ changes depending on the size of Δx. Due to the limitation of CPU power; however, we can calculate the values of $\sqrt{\overline{\delta G^2}}$ for low temperature $T=1$ only for relatively large segment, i.e., $\Delta x=0.1$, 0.5, and 1. Thus, by assuming the relation between Δx and $\sqrt{\overline{\delta G^2}}$ found in Sec. III A, here we have extrapolated the value of $\sqrt{\overline{\delta G^2}}$ for small Δx and found $\ln\sqrt{\overline{\delta G^2}}/\Delta U = -0.15 \log \Delta x/\Delta U - 2.87$. This relation is in accordance with the change of total energy and reaction coordinate for flipping one dipole represented by $\Delta E_{\mathrm{flip}}/N$ and Δx_{flip}. In the 92 dipolar system, we estimate the average solvent-solvent and solute-solvent interaction energies as $\bar{h}=0.27$ and $\bar{g}=-0.01$, and therefore we have $\Delta x_{\mathrm{flip}}=0.02$ and $\Delta E_{\mathrm{flip}}/N=0.06$, respectively. From the extrapolated function, we have $\sqrt{\overline{\delta G^2}}=0.07$ if we regard Δx_{flip} as the segment size. This value is roughly in accordance with $\Delta E_{\mathrm{flip}}/N$, which indicates the changes of energy for flipping dipoles are reflecting the amplitude $\sqrt{\overline{\delta G^2}}$.

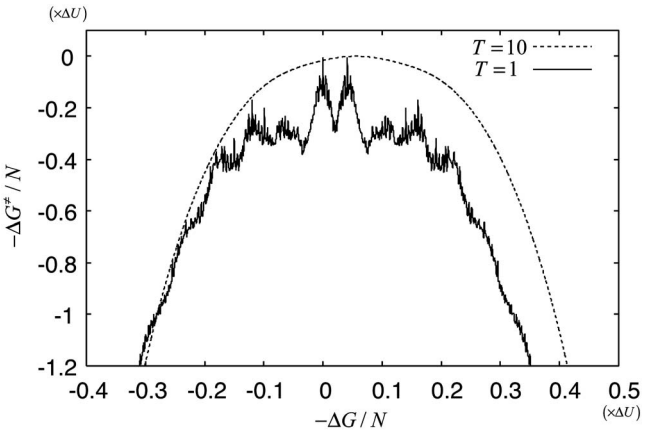

FIG. 9. The energy gap dependence of the activation energy at the temperatures $T=10$ (dashed line) and $T=1$ (solid line) calculated from the energy landscapes with $\Delta x=0.1$.

For a system with large degrees of freedom, the minimal values of Δx can be very small, but, as mentioned in Sec. III A, the energy landscape with the segment size $\Delta x \approx \Delta x_{\mathrm{flip}}$ is of practical importance for reaction process.

C. Energy gap low for ET reaction rates

The free energy landscapes for $G^P(x,T)$ is obtained from $G^R(x,T)$ by using Eq. (1.4). Using the energy landscapes for the 92 dipolar system, we calculate the activation energy $\Delta G^{\neq}$ as the function of energy gap $-\Delta G$. If we denote the minimum values of the reactant and product states as G^R_{min} and G^P_{min}, and express the crossing point of the two surfaces as $x^{\neq}$, we have

$$G^R(x^{\neq},T) - G^R_{\mathrm{min}} = G^P(x^{\neq},T) - G^P_{\mathrm{min}} + \Delta G, \quad (3.9)$$

which allows us to calculate $x^{\neq}$ for fixed ΔG. Since the activation energy $\Delta G^{\neq}$ is given by

$$\Delta G^{\neq} = \{G^R(x^{\neq},T) - G^R_{\mathrm{min}}\}, \quad (3.10)$$

we can depict the energy gap law by plotting $-\Delta G^{\neq}$ as the function of $-\Delta G$.

Figure 9 shows the energy gap dependence of the activation energy at the temperatures $T=10$ (dashed line) and $T=1$ (solid line) calculated from the energy landscapes with the segment size $\Delta x=0.1$, which is slightly larger than Δx_{flip}. All curves of the activation energy are symmetric with respect to the minimum point, since the free energy landscape of the reactant states is the even function. In the low temperature case, $T=1$, the energy gap law exhibits a roughness reflected on the notched structure of the energy landscape. Although the profiles of the roughness may change depending on Δx, the segment size smaller than Δx_{flip} is not necessary to employ for studying the reaction processes. Because the states can only change through the dipolar flipping in the order of Δx_{flip}. Notice that the microscopic profiles of rough-

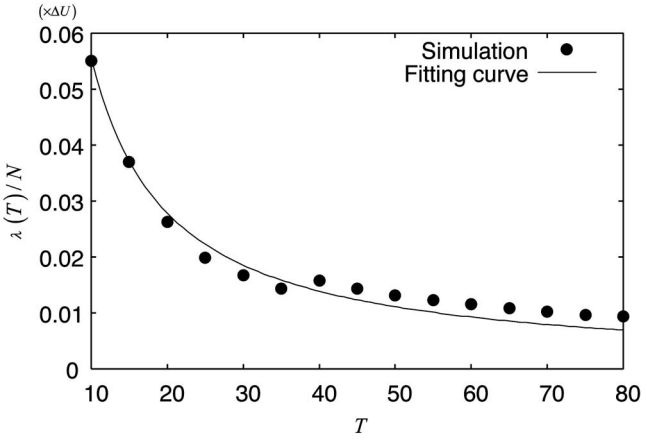

FIG. 10. The reorganization energy, $\lambda(T)$, which gives the minimum activation energy is plotted for different temperatures for $T \geqslant 10$ (dots). The solid line represents the fitting curve, $\lambda(T)=1/4aT$, with $a=4.9\times10^{-3}$.

ness depend on the distribution of the dipolar positions and if we take an ensemble average for different distributions, such small roughness on the activation energy may not be observed.

Due to the nonparabolic shape of energy landscapes, the energy landscapes are not quadratic besides small $|x|$. The calculated energy gap decreases faster than the quadratic function besides the range about $|\Delta G| \leqslant 0.2$. This deviation becomes large for high temperature case, since the free energy landscape becomes steep as explained by Eq. (3.8).

The energy gap low, Eq. (1.1), indicates that the maximum reaction rate depends on the reorganization energy λ. When a temperature rises, the profile of activation energy also shifts to the left for $T \geqslant 10$ as illustrated in Fig. 10. For high temperature case, the free energy landscape can be written as $G^R(x,T) \approx -k_B T \ln n(x)$. Since $n(x)$ is approximated by a temperature-independent Gaussian function for small x, we can express the free energy as

$$G^P(x,T) = aT\left(x - \frac{1}{2aT}\right)^2 + G^P_{\min}, \tag{3.11}$$

where a is some constant and $G^P_{\min}$ satisfies $G^P_{\min}=G^R_{\min} - 1/4aT$. Since the crossing point and the activation energy are expressed as $x^{\neq}=\Delta G+1/4aT$ and

$$-\Delta G^{\neq} = -\frac{((-\Delta G)-\lambda(T))^2}{4\lambda(T)}, \tag{3.12}$$

respectively, the peak position of the activation energy is equal to the reorganization energy $\lambda(T)=1/4aT$. The peak positions of the calculated results are plotted in Fig. 10. These results are well fitted by $\lambda(T)=1/4aT$ with $a=4.9\times10^{-3}$ as illustrated by the solid line in the figure. For studying the solvation saturation effect, Milischuk and Matyushov utilized the relation that the reorganization energy is proportional to $1/T$ for a dipolar solvation system at constant volume.[45] The present results are consistent with their analysis.

IV. CONCLUSION

We calculated the free energy landscape by generating all possible states for a 26 dipolar system and by using the Wang-Landau sampling algorithm for a 92 dipolar system. Using the results from the 26 dipolar system, we analyzed the notched structure of the free energy profiles for different segment sizes of reaction coordinate Δx. The notched part arose due to the difference of the lowest energy state between the segments. The amplitude (the standard deviation) of the notched part $\sqrt{\overline{\delta G^2}}$ increased as the segment size decreased especially for low temperature. The relation between the segment size and the amplitude was in accordance with the relation between the change of reaction coordinate Δx_{flip} and the total energy ΔE_{flip} for flipping a dipole of the system. Although the true free energy landscapes had notched structures whose scale is smaller than Δx_{flip}, a real transition may occur only through the flipping of dipoles and therefore the scale of Δx smaller than that of Δx_{flip} may not affect on the reaction processes.

We analyzed the profiles of energy landscapes in the 92 dipolar system and found that the free energy landscape showed a parabolic shape for the small reaction coordinate region at high temperature as the Marcus theory predicted. In the large reaction coordinate region, the profiles exhibited a nonquadratic shape, since the number of states for such segment region was very few and the distribution of states becomes non-Gaussian. At low temperature, we estimated the amplitude of notched part and compared with Δx_{flip} and ΔE_{flip} for the 92 dipolar system. These values were also in accordance with the relation between Δx and $\sqrt{\overline{\delta G^2}}$. Although we could not calculate $\sqrt{\overline{\delta G^2}}$ for very small Δx, we could evaluate $\sqrt{\overline{\delta G^2}}$ for any Δx with the relation found in the 26 dipolar system. We should mention that the solvent dipoles used in this model are restricted to point toward and opposite to the central solute dipole. This makes a system extremely frustrated and the energy of the solvent dipoles in the equilibrium state becomes much higher than that of a crystal with dipolar orientational relaxation. The free energy landscapes below the freezing temperature may be smoother for a realistic system due to the continuity of rotational motion of a solvent dipole.

Finally, the activation energy as the function of the energy gap was calculated by using the free energy landscape for the 92 dipolar system. At high temperature, the bell shaped reaction rate was observed. Due to the nonquadratic free energy landscape, the nonquadratic dependency appeared as the energy gap increased. Thus the profile of the calculated reaction rate became steeper than that derived from the quadratic free energy landscape. When the temperature decreased, the parabolic profile of activation energy $\Delta G^{\neq}$ also shifted to the lower energy part of $-\Delta G$, since the value of the free energy was proportional to the temperature at the high temperature regime. At low temperature, the profile of the reaction rate became rough due to the notched structure of the free energy landscape. The appearance of roughness depended on the distribution of dipolar positions and if we take an ensemble average for different distribution of dipoles, this roughness may not be observed. In such case,

one should explore dynamical as well as thermal aspects of a system by means of nonlinear response function to separate inhomogeneous and homogeneous contribution of reaction processes.[46] We leave these for future studies.

ACKNOWLEDGMENTS

The authors wish to express their gratitude to A. Yoshimori, K. Ando, and R. Akiyama for helpful discussions. The financial support from a Grant-in-Aid for Scientific Research A 15205005 from the Japan Society for the Promotion of Science and Morino Science Foundation is acknowledged.

[1] R. A. Marcus, Rev. Mod. Phys. **65**, 599 (1993).
[2] R. A. Marcus, J. Chem. Phys. **24**, 966 (1956); **24**, 979 (1956).
[3] J. R. Miller, L. T. Calcaterra, and G. L. Closs, J. Am. Chem. Soc. **106**, 3047 (1984).
[4] M. R. Wasielewski, M. P. Niemczyk, W. A. Svec, and E. B. Pewitt, J. Am. Chem. Soc. **107**, 1080 (1985).
[5] N. Mataga, T. Asahi, Y. Kanda, T. Okada, and T. Kakitani, Chem. Phys. **127**, 249 (1988).
[6] B. Bagchi and A. Chandra, Adv. Chem. Phys. **80**, 1 (1991).
[7] B. U. Felderhof, J. Chem. Phys. **67**, 493 (1977).
[8] R. A. Marcus, Discuss. Faraday Soc. **29**, 21 (1960).
[9] A. Warshel, J. Phys. Chem. **86**, 2218 (1982).
[10] D. F. Calef and P. G. Wolynes, J. Chem. Phys. **78**, 470 (1983).
[11] J. K. Hwang and A. Warshel, J. Am. Chem. Soc. **109**, 715 (1987).
[12] R. A. Kuharski, J. S. Bader, D. Chandler, M. Sprik, M. L. Klein, and R. W. Impey, J. Chem. Phys. **89**, 3248 (1988).
[13] E. A. Carter and J. T. Hynes, J. Phys. Chem. **93**, 2184 (1989).
[14] K. Ando and S. Kato, J. Chem. Phys. **95**, 5966 (1991).
[15] A. Chandra and B. Bagchi, J. Chem. Phys. **91**, 7181 (1989).
[16] A. Chandra and B. Bagchi, J. Chem. Phys. **94**, 2258 (1991).
[17] M. Tachiya, J. Phys. Chem. **93**, 7050 (1989).
[18] A. Yoshimori, T. Kakitani, Y. Enomoto, and N. Mataga, J. Phys. Chem. **93**, 8316 (1989).
[19] R. Zwanzig, J. Chem. Phys. **38**, 2766 (1963).
[20] H.-X. Zhou and B. Bagchi, J. Chem. Phys. **97**, 3610 (1992).
[21] T.-W. Nee and R. Zwanzig, J. Chem. Phys. **52**, 6353 (1970).
[22] A. Papazyan and M. Maroncelli, J. Chem. Phys. **95**, 9219 (1991).
[23] P. G. Wolynes, J. Chem. Phys. **86**, 5133 (1987).
[24] L. E. Fried and S. Mukamel, J. Chem. Phys. **93**, 932 (1990).
[25] S. S. Komath and B. Bagchi, J. Chem. Phys. **98**, 8987 (1993).
[26] H.-X. Zhou, B. Bagchi, A. Papazyan, and M. Maroncelli, J. Chem. Phys. **97**, 9311 (1992).
[27] A. Papazyan and M. Maroncelli, J. Chem. Phys. **102**, 2888 (1995).
[28] J. N. Onuchic and P. G. Wolynes, J. Chem. Phys. **98**, 2218 (1993).
[29] B. Derrida, Phys. Rev. Lett. **45**, 79 (1980).
[30] B. Derrida, Phys. Rev. B **24**, 2613 (1981).
[31] V. B. P. Leite and J. N. Onuchic, J. Phys. Chem. **100**, 7680 (1996).
[32] V. B. P. Leite, L. C. P. Alonso, M. Newton, and J. Wang, Phys. Rev. Lett. **95**, 118301 (2005).
[33] Y. Tanimura, V. B. P. Leite, and J. N. Onuchic, J. Chem. Phys. **117**, 2172 (2002).
[34] Y. Suzuki and Y. Tanimura, J. Chem. Phys. **124**, 124508 (2006).
[35] B. A. Berg and T. Neuhaus, Phys. Lett. B **267**, 249 (1991).
[36] B. A. Berg and T. Neuhaus, Phys. Rev. Lett. **68**, 9 (1992).
[37] B. A. Berg and T. Celik, Phys. Rev. Lett. **69**, 2292 (1992).
[38] U. H. E. Hansmann and Y. Okamoto, J. Comput. Chem. **14**, 1333 (1993).
[39] N. Urakami and M. Takasu, J. Phys. Soc. Jpn. **65**, 2694 (1996).
[40] H. Noguchi and K. Yoshikawa, J. Chem. Phys. **109**, 5070 (1998).
[41] H. Okumura and Y. Okamoto, Chem. Phys. Lett. **391**, 248 (2004).
[42] H. Okumura and Y. Okamoto, Phys. Rev. E **70**, 026702 (2004).
[43] F. Wang and D. P. Landau, Phys. Rev. Lett. **86**, 2050 (2001).
[44] F. Wang and D. P. Landau, Phys. Rev. E **64**, 056101 (2001).
[45] A. Milischuk and D. V. Matyushov, J. Phys. Chem. A **106**, 2146 (2002).
[46] Y. Tanimura, H. Takano, and J. Klafter, J. Chem. Phys. **108**, 1851 (1998).